Screen Identifies DYRK1B Network as Mediator of Transcription Repression on Damaged Chromatin

Chao Dong[1], Kirk L. West[2], Xin Yi Tan[1], Junshi Li[1], Toyotaka Ishibashi[3], Cheng-han Yu[1], Shirley M.H. Sy[1], Justin W.C. Leung[2,#], Michael S.Y. Huen[1,4,#]

[1]School of Biomedical Sciences, LKS Faculty of Medicine, The University of Hong Kong, 21 Sassoon Road, Pokfulam, Hong Kong S.A.R.;
[2]Department of Radiation Oncology, College of Medicine, University of Arkansas for Medical Sciences, Little Rock, AR 72205, USA;
[3]Division of Life Science, Hong Kong University of Science and Technology, Clear Water Bay, N.T., Hong Kong S.A.R.;
[4]State Key Laboratory of Brain and Cognitive Sciences, The University of Hong Kong, 5 Sassoon Road, Pokfulam, Hong Kong S.A.R.
[#]correspondence: Michael S.Y. Huen huen.michael@hku.hk; Justin W.C. Leung jwleung@uams.edu

DNA double-strand breaks (DSBs) trigger transient pausing of nearby transcription, an emerging ATM-dependent response that suppresses chromosomal instability. We screened a chemical library designed to target the human kinome for new activities that mediate gene silencing on DSB-flanking chromatin, and have uncovered the DYRK1B kinase as an early respondent to DNA damage. We showed that DYRK1B is swiftly and transiently recruited to laser microirradiated sites, and that genetic inactivation of DYRK1B or its kinase activity attenuated DSB-induced gene silencing and led to compromised DNA repair. Notably, global transcription shutdown alleviated DNA repair defects associated with DYRK1B loss, suggesting that DYRK1B is strictly required for DSB repair on active chromatin. We also found that DYRK1B mediates transcription silencing in part via phosphorylating and enforcing DSB accumulation of the histone methyltransferase EHMT2. Together, our findings unveil the DYRK1B signalling network as a key branch of the mammalian DNA Damage Response circuitries, and establish the DYRK1B-EHMT2 axis as an effector that coordinates DSB repair on transcribed chromatin.

Significance Statement

Cells avoid clashes between DNA repair machineries and the transcription apparatus by temporary halting gene expression in the vicinity of DNA double-strand breaks (DSBs), an emerging DNA Damage Response (DDR) that underlies genome integrity protection. In this study we screened for novel activities that may be important in this DDR and have identified the DYRK1B kinase as a new component of the mammalian DDR that specialises in finetuning DSB repair on the actively transcribed chromatin. Moreover, global analysis of DYRK1B substrates has led to the identification of the histone methyltransferase EHMT2 as a DYRK1B target and effector. Our findings uncover the DYRK1B network as a new DDR sub-pathway that preserve the integrity of the active chromatin.

Introduction

Repair of DNA double-strand breaks (DSBs) is accompanied by change in local chromatin architecture and its ongoing transactions, including transcription [1]. Indeed, cells halt gene expression on the DSB-flanking chromatin to prevent collision between the DNA repair machinery and the transcription apparatus, which in turn facilitates DNA repair and suppresses chromosomal instability [2]. In this regard, the apical DNA damage kinase ATM targets a multitude of chromatin-modifying activities [3-5] and plays multifaceted roles to establish a DSB microenvironment to suppress local transcription [6]. Interestingly, the DNA-dependent protein kinase (DNA-PK) complex has also been reported to arrest transcription [7] via proteasome-dependent eviction of RNAPII [8], although whether ATM and DNA-PK activities intercept remains undefined. Moreover, while transcription suppression on DSB-flanking chromatin also requires a growing number of chromatin remodellers and transcription regulators [9-13], it is currently enigmatic how DSB signals are propagated and translated to fine-tune local transcriptional activities to effect DNA repair processes.

DYRK1B (a.k.a. MIRK) is a member of the evolutionarily-conserved family of DYRK kinases, and encodes a dual-specificity serine/threonine protein kinase with implicated roles in cell differentiation and survival [14, 15]. DYRK1B is upregulated in human cancers, and several lines of evidence have shown that DYRK1B maintains cancer cells in their quiescent state to confer chemoresistance [16, 17], and that pharmacological inhibition of its kinase activity may offer a means to sensitise cells to the cytotoxic effects of anti-cancer therapeutics [18]. Aside its putative oncogenic properties, DYRK1B is also involved in gene transcriptional control in growth and development [19], and that genetic mutations are causally linked with an inherited form of metabolic syndrome [20]. Notably, while DYRK1B inactivation may contribute to genome instability [21], and that it has been reported to reside in DSB repair macromolecular protein complexes in a proteomic study [22], a role of DYRK1B in DNA damage response control is not known.

Results

Chemical screen identifies DYRK1B as a novel activity required for transcription suppression on DSB-flanking chromatin

To isolate novel activities that orchestrate DSB repair on transcribed chromatin, a kinase inhibitor library consisting of 760 compounds were examined for their effect on DSB-induced transcription suppression. To this end we took advantage of a previously established transcription reporter wherein nascent transcriptional activities can be monitored by local YFP-MS2 accumulation [23]. Proximal DSBs can be induced by 4-hydroxytamoxifen (4-OHT) and Shield-1, which promote the docking of the ER-fused FokI-mCherry-LacI nuclease onto LacO arrays (x256) located upstream of the transcriptional unit, to ensue transcription suppression (**Figure 1A**). Accordingly, DSBs were induced in reporter cells pre-treated with individual kinase inhibitors, which were subjected to high-content microscopy and automated analyses of cells positive for YFP-MS2 foci (**Figure 1B**). Consistent with a pivotal role of ATM in orchestrating DSB responses [24], including DSB-induced transcription silencing *in cis* (DISC)[6], chemical inhibitors that targeted the ATM kinase compromised DISC, as reflected by the high percentages of cells with YFP-MS2 foci (**Figure 1C; SI Appendix, Figure S1 & Dataset S1**). We filtered out kinase targets that reside in the cytoplasm (**SI Appendix, Figure S1A**), and amongst the list of nuclear kinase targets we were drawn to DYRK1B (**Figure 1C; SI Appendix, Figure S1B**) as it was recently reported to interact with the DSB response factor RNF169 [22]. We confirmed that chemical inhibition of DYRK1B, much like that of ATM, attenuated DSB-induced transcription suppression (**Figure 1D**), and that nascent transcription can be inhibited by the transcription elongation inhibitor 5,6-dichlorobenzimidazole 1-β-D-ribofuranoside (DRB) (**SI Appendix, Figure S2A**). In support of the idea wherein DYRK1B may encode an ATM effector in mounting transcription suppression on the damaged chromatin, we found that chemical inhibition of both ATM and DYRK1B compromised DISC to the same extent as that observed in ATMi-treated cells, suggesting that ATM and DYRK1B may be epistatic in this DDR (**Figure 1E**).

DYRK1B promotes DISC in a kinase-dependent manner

To corroborate that DYRK1B is important in transcription suppression on the damaged chromatin, we depleted DYRK1B using two independent small interference RNAs (siRNAs) (**SI Appendix, Figure S2B**), and found that DYRK1B silencing led to sustained transcription despite DSB induction in the U2OS-DSB reporter cells (**Figure 2A**). Similar observations were made in cells lenti-virally transduced with two independent DYRK1B-targeting guide RNAs (gRNAs) (**SI Appendix, Figure S2B & S2C**). Moreover, in stark contrast to control cells, we found that DYRK1B-inactivated cells failed to suppress 5-ethynyl uridine (5-EU) incorporation at laser microirradiated sites (**Figure 2B – C; SI Appendix, Figure S2D**), indicating that DYRK1B is required to inhibit nascent transcription at DNA damage sites. Given that chemical inhibition of ATM or DYRK1B attenuated suppression of 5-EU incorporation at laser-induced DSBs (**SI Appendix, Figure S2E**), we genetically examined whether DYRK1B kinase activity is important in DISC by reconstituting DYRK1B-depleted cells with wildtype DYRK1B or its kinase inactive mutants K140M and D239A [25, 26]. In line with the requirement of DYRK1B kinase activity in suppressing transcription on the damaged chromatin, mutational inactivation of DYRK1B catalytic activity compromised DISC in reporter cells (**Figure 2D**) as well as in laser micro-irradiated cells (**SI Appendix, Figure S2F**). Together, these data firmly establish the DYRK1B kinase as a novel transcription control factor at DSBs.

DYRK1B promotes DISC-associated histone ubiquitylation and RNAPII dynamics

Given that ATM mounts DISC by promoting local H2A ubiquitylation [6] we tested whether chemical inhibition of DYRK1B may similarly compromise DSB-associated histone ubiquitylation. Consistently, DYRK1B inactivation led to marked reduction in H2A ubiquitylation, but did not noticeably affect levels of total ubiquitin conjugates (FK2) or K63-linked ubiquitin adducts at FokI-induced DSBs (**SI Appendix, Figure S3A – S3C**). Moreover, in line with a role in regulating RNAPII-dependent transcriptional activities on the damaged chromatin, DYRK1B inhibition led to sustained accumulation and phosphorylation of RNAPII at FokI-induced DSBs in the U2OS-DSB reporter cells (**SI Appendix, Figure S3D – S3G**). Together, these findings suggest that DYRK1B may regulate transcriptional activities at DSBs in an epistatic manner with ATM.

DYRK1B is recruited to DSBs

We next examined whether DYRK1B may play a direct role on DSB-flanking chromatin. To this end we tested whether DYRK1B may be mobilised in response to DNA damage. Intriguingly, we found that laser microirradiation triggered swift and transient accumulation of GFP-tagged DYRK1B at DNA damage tracks (**Figure 3A**). To decipher how DYRK1B docks at DSBs we generated a panel of DYRK1B deletion mutants and analysed their ability to accumulate at laser-induced DNA damage tracks (**Figure 3B - C**). Interestingly, we found a strict requirement of the DYRK1B kinase domain in supporting its accumulation at DSBs (**Figure 3D; SI Appendix, Figure S4A**), and that its kinase domain (KD) itself suffices in docking at laser-induced DNA damage tracks (**Figure 3B & E**). To examine if kinase activity is required for DYRK1B DSB accumulation, we monitored the dynamics of DYRK1B kinase inactive mutants (i.e. K140M and D239A) at laser-induced DNA damage tracks. In contrast to the kinase domain deletion mutant, GFP-DYRK1B K140M and D239A displayed robust accumulation at laser microirradiated sites (**SI Appendix, Figure S4B**), suggesting that DYRK1B kinase activity *per se* is not a pre-requisite for its recruitment to DSBs.

Given that PARP plays an early role in mobilising early respondents to DSBs [27], we chemically inhibited PARylation using Olaparib and examined whether DYRK1B accumulation at laser-induced DNA damage tracks requires PARP activity. We also pre-treated cells with ATM- and ATR-specific inhibitors to explore whether these master regulators of DDRs are necessary for DYRK1B docking on the damaged chromatin. Accordingly, while GFP-DYRK1B accumulation at laser-induced DSBs was only marginally attenuated in ATM/ATR-inhibited cells, PARP inhibition completely precluded DYRK1B from concentrating at DNA damage sites (**Figure 3F; SI Appendix, Figure S4C**). Inhibiting ATM and ATR, on the other hand, led to substantial delay in GFP-53BP1 recruitment to laser microirradiated sites (**SI Appendix, Figure S4D**). Noting that DYRK1B is endowed with transcription regulatory roles on DSB-flanking chromatin, we also tested whether global transcription suppression may impact its migration to DSBs. Interestingly, chemical inhibition of transcription using a panel of small molecules that target different components of the host transcription apparatus led to quantitative attenuation of DYRK1B accumulation at DSBs (**Figure 3G; SI Appendix, Figure S4E**). These data led us to postulate that DYRK1B may preferentially target DSBs on transcribed chromatin.

DYRK1B facilitates DSB repair

Our observations that DYRK1B promotes transcription silencing on DSB-flanking chromatin prompted us to test whether DYRK1B kinase may be required for efficient DNA repair. To this end we measured DNA repair kinetics following cell exposure to ionising radiation (IR) using the Comet assay. In support of a role of DYRK1B in DSB repair, IR-induced DNA damage persisted in DYRK1B-inactivated cells (**SI Appendix, Figure S5A**). Moreover, expression of wildtype DYRK1B but not its kinase inactive mutants alleviated the DNA repair defect in DYRK1B-silenced cells (**Figure 4A**), highlighting a role of its kinase activity in orchestrating DSB repair processes. To consolidate a role of DYRK1B in DSB repair, we further analysed chromosome stability by scoring chromosome breaks in DYRK1B-deficient cells following IR treatment. Consistently, we found that DYRK1B promotes repair of IR-induced chromosome breaks (**SI Appendix, Figure S5B**), and that its kinase activity is similarly required for recovery from IR treatment (**Figure 4B**). Together, these data implicate DYRK1B-dependent transcription silencing as a key event that finetunes DSB repair.

Global transcription shutdown alleviates DNA repair defects in DYRK1B-inactivated cells

That DYRK1B may preferentially target DSBs on transcribing chromatin (**Figure 3G; SI Appendix, Figure S4E**) and is important for efficient DNA repair led us to speculate whether the kinase may facilitate repair of DSBs within transcriptionally active chromatin. We explored this possibility by performing both the Comet assay (**Figure 4C**) and by scoring chromosome breaks (**Figure 4F**) with IR-challenged cells pre-treated with the transcription inhibitor DRB. Notably, global transcription shutdown not only alleviated the DNA repair defect associated with DYRK1B loss (**Figure 4D - E**) but also suppressed chromosome breaks in otherwise DYRK1B-inactivated cells (**Figure 4G**). Together, these data suggest that DYRK1B may facilitate repair of DSBs by orchestrating local transcriptional activities.

Phospho-analysis of DYRK1B substrates identifies novel DISC factors

Given the requirement of DYRK1B kinase activity in orchestrating DSB-induced transcription silencing and in DNA repair, we performed a global profiling of DYRK1B targets with the aim to delineate how DYRK1B mediates these DSB responses (**Figure 5A**). We sampled and enriched phosphopeptides obtained from parental RPE-1 cells, as well as DYRK1B over-expressing and DYRK1B-inactivated counterparts. Accordingly, bioinformatic analyses of phospho-peptides revealed high degree of overlaps between parental RPE-1 cells and those that over-express DYRK1B, as well as those between the two isogenic DYRK1B gRNA-targeted cell lines (**SI Appendix, Figure S6A**). Notably, analysis of phospho-peptides that are significantly enriched in cells with ectopic expression of DYRK1B (OE) over its knockout counterparts (KO1+KO2) (**Figure 5B; SI Appendix, Dataset S2**) uncovered that DYRK1B preferentially targets substrates on the S/TP motif (**Figure 5C**). Furthermore, Gene Ontology (GO) enrichment analysis of putative DYRK1B targets indicated that DYRK1B may be involved in a plethora of biochemical pathways, including those that regulate transcription (**Figure 5D; SI Appendix, Figure S6B & Dataset S3A-S3C**).

With a focus to decipher how DYRK1B mediates DISC we selected a number of candidates from transcription-related pathways (**Figure 5D; SI Appendix, Figure S6C & Dataset S3A-S3C**) and performed an RNAi-based validation screen to isolate novel players that are important in transcription suppression on the damaged chromatin (**Figure 5E**). Amongst those that are required for DISC, we were drawn to EHMT2 (a.k.a. G9a) as it has established roles in gene repression [28], and represents a promising drug target for cancer [29]. More recently, EHMT2 has also been implicated in cell responses to DNA damage [30-32]. Accordingly, we confirmed the DYRK1B-EHMT2 interaction using a co-immunoprecipitation approach (**SI Appendix, Figure S7A**), and that DYRK1B promotes EHMT2 phosphorylation in a kinase-dependent manner (**SI Appendix, Figure S7B**).

EHMT2 promotes transcription silencing on damaged chromatin

In line with a requirement of EHMT2 in pausing transcriptional activities proximal to FokI-induced DSBs in U2OS-DSB reporter cells (**Figure 5E & Figure 6A**), genetic inactivation of EHMT2 also led to sustained 5-EU incorporation at laser-induced DNA damage tracks (**Figure 6B**). Given that EHMT2 is endowed with histone lysine methyltransferase activity [28] we chemically inhibited EHMT2 using UNC0638 to examine if its catalytic activity may be required for transcription suppression on DSB-flanking chromatin [33, 34]. Indeed, chemical inhibition of EHMT2 led to sustained nascent transcription at FokI-induced DSBs as well as at laser-induced DNA damage tracks (**Figure 6C – D**). To further corroborate a role of EHMT2 activity in DISC we reconstituted EHMT2-inactivated cells with either wildtype EHMT2 or its catalytic mutant (ΔSET), and assayed if its methyltransferase activity is required for transcription silencing at FokI- and laser-induced DSBs. In line with a requirement of EHMT2 activity in DISC, re-expression of wildtype EHMT2 but not its ΔSET mutant in EHMT2-inactivated cells restored transcription suppressing following DSB induction (**Figure 6E – F**). Together, these data establish the histone methyltransferase EHMT2 as an important activity in mounting DISC.

DYRK1B promotes EHMT2 accumulation at DSBs

To further explore how DYRK1B may effect DISC via EHMT2 phosphorylation we first examined if EHMT2 recruitment to DSBs may depend on DYRK1B. Time-lapse imaging of GFP-EHMT2 following laser microirradiation indicated that DYRK1B enforces EHMT2 accumulation at DSBs, as GFP-EHMT2 recruitment was quantitatively attenuated in DYRK1B-inactivated cells (**Figure 7A**) as well as in DYRK1B-inhibited cells (**SI Appendix, Figure S7C**), although DYRK1B deficiency did not noticeably alter EHMT2 protein expression level (**SI Appendix, Figure S7D**). Moreover, similar to those that underlie DYRK1B recruitment to DSBs, EHMT2 deposition at DSBs required PARP and transcriptional activities (**SI Appendix, Figure S7C**). These findings prompted us to investigate whether DYRK1B may promote EHMT2 deposition at DSBs via its phosphorylation. To this end we generated EHMT2 phospho-mutants (i.e. T346A and T346D) according to the DYRK1B-enriched EHMT2 phospho-peptide (**Figure 7B – C; SI Appendix, Dataset S3C**), and examined their migration kinetics to laser-induced DSBs. Notably, while the non-phosphorylatable T346A mutation partially hampered EHMT2 recruitment to DSBs, the phospho-mimicking T346D mutant accumulated with much more robust kinetics when

compared to wildtype EHMT2 (**Figure 7D**). These data suggest that DYRK1B facilitates EHMT2 docking at DSBs, at least in part, via targeted T346 phosphorylation.

Discussion

In this study we have uncovered the DYRK1B network as a branch of mammalian DDR pathways that orchestrates transcriptional activities on the damaged chromatin for effective DNA repair (**Figure 7E**). By conducting a kinase inhibitor library screen we identified DYRK1B as a S/TP-targeting kinase that accumulates at DSBs to promote transcription suppression on DSB-flanking chromatin. Phospho-profiling of DYRK1B substrates further unveiled that DYRK1B-dependent DISC is, at least in part, effected via EHMT2 phosphorylation and its docking at DSBs. Our findings thus highlight the DYRK1B kinase as a specialised mediator of ATM-dependent DDRs that serves to maintain genome stability of transcribed chromatin.

Our appreciation for the interplay between DSB metabolism and local transcriptional activities has grown since the introduction of elegant platforms in which DSBs can be induced at specific genomic loci [6, 7, 35-37], thus permitting the study of DSB microenvironment (e.g. histone marks) and its impact on local chromatin transactions [38, 39]. Notably, it has now become evident that DSB repair can be dynamic [40, 41], and that DSB signal output is limited by local chromatin architecture and activities [36, 42]. In particular, the molecular events that underlie transcriptional control on damaged chromatin has garnered much interest [11, 36, 42, 43], in part due to its emerging impact on genome stability and its relevance to human diseases. In this connection, seeing that DYRK1B has been associated with a metabolic syndrome [20] we subcloned the clinically-derived DYRK1B mutations (i.e. H90P and R102C) and have examined their impact on DYRK1B-dependent DDRs (**SI Appendix, Figure S8**). Intriguingly, while both DYRK1B mutations compromised DSB repair in the Comet assay (**SI Appendix, Figure S8A**), R102C exhibited perturbed DSB recruitment kinetics (**SI Appendix, Figure S8B**), and failed to suppress transcription following FokI- and laser-induced DSBs (**SI Appendix, Figure S8C – D**). Given the emerging links between DSB repair and metabolic homeostasis [44] it would be of significant interest to explore how defective DISC may impact cell differentiation and tissue homeostasis.

Global phospho-profiling of DYRK1B targets led to the uncovering of the histone lysine methyltransferase EHMT2 as one of the candidate downstream effectors that promotes DSB-induced transcription silencing (**Figure 5**). Indeed, that EHMT2 plays established roles in gene repression [28] suggested that the DYRK1B-EHMT2 axis may represent a novel branch of DDRs with specialised roles in preserving the transcriptionally-active chromatin. In line with this notion, we found that DYRK1B targets EHMT2 at a highly-conserved S/TP motif (**Figure 7B**), and that EHMT2 carrying the phospho-mimetic T346D mutation much more readily accumulated at laser-induced DSBs (**Figure 7D**), suggesting that DYRK1B may promote EHMT2 docking and activity at DSBs. While the mechanistic details that underlie EHMT2-dependent DISC remains to be defined, that both chemical inhibition or genetic inactivation of EHMT2 methyltransferase activity led to sustained nascent transcription at the damaged chromatin (**Figure 6C – F**) suggest that EHMT2 may exert gene repression by contributing to the local DSB microenvironment, potentially by targeting histone molecules.

Our observation that a number of putative DYRK1B targets may be important in transcription suppression on DSB-flanking chromatin (**Figure 5E**) suggests that DYRK1B may orchestrate DSB repair on transcriptionally-active chromatin via multipartite mechanisms. To further explore this possibility we examined whether DYRK1B may support DSB recruitment of chromatin remodelling complexes and chromatin architectural factors recently implicated in DISC [3, 10]. Notably, we found that DYRK1B deficiency impinged on, to varying extent, migration of PBAF (i.e. BRD7 and BAF180) and cohesin (i.e. STAG2) subunits to laser-induced DNA damage tracks, but not that of the polycomb repressive complex components BMI1 and EZH2 (**SI Appendix, Figure S9**). On the other hand, DYRK1B appears to have minimal impact on DSB accumulation of negative elongation factors NELF-A/E (**SI Appendix, Figure S10**) and did not detectably affect the metabolism of R-loops (**SI Appendix, Figure S11**). Together, while DYRK1B likely effects transcription suppression via multiple targets on the DSB-flanking chromatin, the fact that DYRK1B-associated DSB repair defects can be alleviated by global transcription inhibition (**Figure 4C – G**) establishes DYRK1B and its network as key signalling intermediates that

promote DISC, a dedicated ATM-dependent DSB response that has evolved to suppress chromosomal instability and maintain gene expression programmes important in cell proliferation and organismal development. We await further work to decipher how DYRK1B coordinates local transcription during DSB metabolism and how it translates to DSB repair and maintenance of chromosome stability.

Materials and Methods

Cell lines, cell culture, plasmids and chemicals

HeLa, U2OS, hTERT RPE-1 and HEK293T cells were cultured in Dulbecco's modified eagle medium (DMEM) containing with 10% fetal bovine serum and 1% penicillin-streptomycin (Gibco, Thermo Fisher Scientific) at 37°C in 5% CO_2. Details to chemicals, plasmids and antibodies are in **Table S1, Table S2** and **Table S3**, respectively.

RNA interference

Cells were transfected twice at 24 hr intervals with either non-targeting control or gene-specific siRNAs (Dharmacon) using Oligofectamine (Invitrogen) according to the manufacturer's instructions. Sequences of siRNAs are listed in **Table S4**.

Lentiviral particle packaging and transduction

HEK293T cells were transiently co-transfected with lentiviral-based expression plasmids, psPAX2 and pMD2.G at the ratio of 4:3:1 using polyethyleneimine (PEI) to produce lentiviral particles. Forty-eight hours after transfection, supernatants containing lentiviruses were filtered with Acrodisc 25 mm Syringe Filter with 0.45 μM membrane (PALL Life Sciences) and were used for cell transduction in the presence of 8 μg ml^{-1} polybrene (Sigma-Aldrich).

Genome editing using the CRISPR-Cas9 method

Gene-targeting gRNAs were subcloned into LentiCRISPR v2 vector (Addgene #52961) following standard procedures. Viral particles containing gRNAs were applied to recipient cells twice at 24 hr intervals in the presence of 8 μg ml^{-1} polybrene (Sigma-Aldrich). Transduced cells were pooled and were selected with DMEM supplemented with 1 μg ml^{-1} puromycin (Sigma-Aldrich) for 1 week. Gene-edited cells were validated by Western Blotting. Sequences of gRNAs are listed in **Table S5**.

Western blotting and Co-immunoprecipitation

Cells were harvested and lysed with NETN buffer [20 mM Tris·HCl (pH 8.0), 100 mM NaCl, 0.5% Nonidet P40, and 1 mM EDTA] supplemented with Benzonase nuclease (ChemCruz) for 30 min on ice. Whole cell lysates were boiled in SDS loading buffer, resolved on SDS-PAGE, transferred to PVDF membranes, and immunoblotted with indicated antibodies. For co-immunoprecipitation, cells were lysed with NETN buffer for 30 min on ice. After centrifugation at 15,000 rpm for 15 min at 4°C, supernatants were incubated with 200 μl streptavidin-conjugated beads (GE Healthcare, Sigma-Aldrich) for 4 hr at 4°C with gentle rotation. Protein-bound beads were washed with ice-cold NETN buffer three times and were subjected to immunoblotting.

Denaturing immunoprecipitation (IP)

HEK293T cells transiently co-transfected with S protein-Flag-Streptavidin-binding peptide (SFB)-tagged EHMT2 mutants with myc epitope-tagged vector or myc epitope-tagged DYRK1B were lysed with denaturing buffer [20 mM Tris·HCl (pH 8.0), 50 mM NaCl, 0.5% Nonidet P40, 0.5% SDS, 0.5% deoxycholate and 1 mM EDTA] on ice for 15 min and subsequently boiled at 95°C for 5 min. The cell lysates were cooled down on ice for 5 min and incubated with Anti-Flag Affinity Gel (Bimake.com) for 3 hr at 4°C with gentle rotation. Protein-bound beads were washed with ice-cold denaturing buffer four times and were boiled with SDS-PAGE sample loading buffer before subjected to immunoblotting.

Immunofluorescence

Cells cultured on coverslips were processed and at indicated time points washed with ice-cold 1× PBS twice and were thereafter fixed with 3% paraformaldehyde for 30 min at room temperature. Cells were subsequently permeabilized with 0.5% Triton for 30 sec after two PBS washes. Coverslips were blocked with 5% milk before incubating with primary antibodies for 1 hr at room temperature. Cells were then washed twice with PBS and were incubated with secondary antibodies for 40 min. Nuclei were counterstained with 4',6-diamidino-2-

phenylindole (DAPI) for 10 sec before coverslips were mounted with fluorescence mounting medium (Dako, Agilent) onto glass slides. Images were acquired by Olympus BX51 fluorescence microscope (UPlanSApo 40×/0.95 objective).

Laser microirradiation and live cell imaging

Laser microirradiation was carried out on an inverted two-photon microscope (LSM780, Carl Zeiss) equipped with an inverted Axio Observer.Z1 stand, motorised scanning stage and an integrated laser microbeam system, with total UV laser output set to 750nm (8%). Cells cultured on glass-bottomed confocal dishes (SPL life Sciences) were subjected to laser microirradiation in a temperature-controlled (37°C) environmental chamber supplied with 5% CO_2 at 24 hr after transient transfection with GFP-tagged indicated plasmids. Time-lapse images were acquired by ZEN 2012 (Carl Zeiss) software with a Plan-Apochromat 40×/1.4 oil DIC M27 objective and were further processed by the ImageJ software to analyse mean fluorescence intensity (MFI) across the laser micro-irradiated regions. MFI was quantified as the difference between the average fluorescence intensity in the laser micro-irradiated regions versus the average fluorescence intensity from adjacent undamaged regions of the same size in the same nucleus.

5-ethynyl uridine (5-EU) incorporation assay

Nascent transcription at laser microirradiated sites was detected by Click-iT™ RNA Alexa Fluor™ 594 Imaging Kit (C10330, Thermo Fisher Scientific). Briefly, cells grown on glass-bottomed confocal dishes (SPL life Sciences) for 24 hr were subjected to laser microirradiation by live Carl Zeiss LSM780 inverted confocal microscope (10× objective) with a 750 nm laser (8% output). Subsequently, cells were cultured with complete media containing 1 mM 5-EU for 1 hr after laser microirradiation. 5-EU labelling was performed following manufacturer instructions. Cells were immunostained for γH2AX and nuclei were counterstained with DAPI before mounting. Images were captured by Olympus BX51 fluorescence microscope (PlanApo N 60×/1.42 Oil-immersion objective). ImageJ was used to analyse relative fluorescence intensity across the laser microirradiated stripes. An analysing line drawn by a line tool was perpendicular to the damaged stripes, centered at the stripes with two ends at undamaged regions and the fluorescence intensity was multi-plotted. Relative fluorescence intensity was normalised to each end from the same cell.

Chromosomal aberration analysis

Chromosomal aberrations were analysed by chromosome metaphase spreading. Cells were cultured in media containing 1 μg ml^{-1} colcemid (KaryoMAX™ Colcemid™ Solution in HBSS, Thermo Fisher Scientific) for 3 hr after 2Gy irradiation and were suspended in 0.8% sodium citrate for 15 min at 37°C. Subsequently, freshly prepared fixative solution (methanol/ acetic acid = 3:1 (v/v)) was added and incubated for 5 min at 37°C. After washing three times by the fixative solution, cells resuspended in a small volume of fixative solution were dropped onto alcohol-cleaned slides and were air-dried. Cells were stained with DAPI before mounting. Images were captured by Nikon Ti2-E Widefield Confocal Microscope (100× oil-immersion objective) using MetaMorph Microscopy and Image Analysis Software (Molecular Devices).

Neutral comet assay

Cells were harvested and resuspended at 5×10^5 cells ml^{-1} in ice cold Ca^{2+}/Mg^{2+} free PBS. Dilute cells were fixed with 37°C molten low melting agarose (LMAgarose, Trevigen) at a ratio of 1:10 (v/v) and cell suspensions (60 μl) were transferred onto prewarmed comet slides (CometSlide, Trevigen). Slides were kept at 4°C in the dark for 30 min, and were immersed in prechilled lysis buffer (2.5 M NaCl, 100 mM EDTA, 10 mM Tris-HCL, 1% N-Lauroylsarcosine sodium, 1% Triton X-100) for 1hr at 4°C followed by further immersion in freshly prepared alkaline buffer for 30 min. Slides were washed with 1×TBE buffer (90 mM Tris, 90 mM boric acid, 3 mM EDTA) twice and were thereafter subjected to TBE electrophoresis at 60 Volt for 5 min. Slides were then fixed in 100% ethanol for 5 min, air-dried and stained with 1 μg ml^{-1} propidium iodide (Sigma-Aldrich) at room temperature in dark for 20 min. Images were captured by Olympus BX51 fluorescence microscope (20× objective). Tail moment of comets were quantified by the ImageJ software with OpenComet plugin.

Kinase inhibitor library screen
Kinase inhibitor library was purchased from Selleck Chemicals. U2OS-DSB reporter cells (kind gift from Dr. Roger Greenberg) were used to assay transcription repression following DSB induction [23]. DSBs were induced by cell pretreatment with shield-1 and 4-OHT, which promote the nuclear translocation of the FokI-mCherry-LacI nuclease and its docking at the LacO transgene array. Nascent transcription at the reporter gene can be monitored by local accumulation of YFP-MS2 upon the addition of 1 μg ml^{-1} doxycycline. U2OS-DSB reporter cells in 96-well microplates (PerkinElmer) were individually incubated with 10 μM kinase inhibitor for 3 hr. Cells were fixed and were subjected to high-content imaging system (IN Cell Analyzer 6500HS). DMSO and ATM inhibitor (KU-55933) were used as negative and positive controls, respectively. Data were processed by IN Carta Analysis Software.

Customised siRNAs screen
Customised siRNAs (3 siRNAs per gene target) were purchased from GenePharma to silence selected putative DYRK1B substrates for a role in DSB-induced transcription repression. U2OS-DSB reporter cells were transfected twice at 24 hr intervals with either non-targeting control or gene-specific siRNAs, and local transcription was monitored by accumulation of YFP-MS2 at the LacO transgene array.

Cell culture and induction of DYRK1B for phospho-proteomic analysis
Parental RPE-1, doxycycline-inducible DYRK1B-overexpressing RPE-1 tetracycline response element (TRE)-DYRK1B, RPE-1-DYRK1B-control, CRISPR/Cas9-mediated RPE-1 DYRK1B-KO#1, and RPE-1 DYRK1B-KO#2 were cultured in DMEM supplemented with 10% fetal bovine serum and 1% Penicillin and Streptomycin. RPE-1 TRE-DYRK1B-SFB cells were induced with 1 μg ml^{-1} doxycycline for 36 hr prior to harvesting. Cells were harvested by trypsin, washed with PBS, flash frozen and stored at -80°C until needed.

Chloroform Methanol Extraction and Generation of TMT-labeled Tryptic Peptides
Frozen cell pellets were thawed on ice and resuspended in lysis buffer (2% SDS, 100 mM Tris-HCl pH 7.6) supplemented with fresh protease and phosphatase inhibitors (Pierce) and incubated on ice for 20 min. Viscosity of the samples was reduced using QIAshredders (Qiagen). Briefly, the lysed samples were applied to the QIAshredder spin column and centrifuged at 16,000 x g for 5 min. Protein concentration within the flowthrough was then quantified using a BCA protein assay (Pierce). Volumes equivalent to 300 μg protein were aliquoted into a fresh 1.5 mL tube and volume adjusted to 100 μL using lysis buffer. Proteins were reduced by addition of TCEP to a final concentration of 5 mM for 30 min at 37°C. The free cysteine residues were alkylated by incubating with 10 mM iodoacetimide for 30 min protected from light. Proteins were then extracted by chloroform methanol extraction with modification [45]. Briefly, 400 μL of methanol was added and the sample was vortexed, followed by 100 μL of chloroform and vortexed. 300 μL of H_2O were added and vortexed. The samples were centrifuged for 1 min at 14,000 x g. The aqueous layer was removed and 400 μL of methanol was added followed by vortexing. The samples were centrifuged at 20,000 x g for 5 min and as much supernatant was possible was removed. The samples were then dried in a SpeedVac. The samples were then resuspended in 300 μL of 100 mM Triethylammonium bicarbonate (TEAB) and sequencing grade trypsin (Promega) in a protein:trypsin ration of 50:1. Samples were tryptically digested overnight at 37°C. The following day the samples were acidified to 0.1% formic acid. Acidified samples were desalted using a Water's C18 Sep-PaK and dried using a SpeedVac. Dried peptide samples were resuspended in 100 μl 100 mM TEAB. 120 μg of peptide for each sample was used for labeling and 10 μL of each sample was combined to create a pooled sample for normalization between batches. 11-plex TMT labels were equilibrated to room temperature and centrifuged prior to resuspension in 60 μL acetonitrile. 30 μL of TMT label was added to a unique sample and incubated at room temperature for 1 hr. The labeling reaction was quenched by addition of 8 μL 5% hydroxylamine and incubation for 15 min at room temperature. 5 μl of each labeled sample were combined and analyzed by mass spectrometry to check for proper mixing. Mixing was adjusted according to the results and the combined samples were desalted by Waters C18 Sep-Pak and dried by SpeedVac.

Phosphopeptide Enrichment and bHPLC- offline fractionation of TMT-labeled Peptides
Pooled TMT-labeled, tryptic peptides previously dried by SpeedVac were resuspended in phosphopeptide binding/wash buffer from the High-Select TiO_2 Phosphopeptide Enrichment Kit (Pierce) and processed for enrichment. The flowthrough from the TiO_2 column was applied to a second phosphopeptide enrichment kit, the High-Select Fe-NTA Phosphopeptide Enrichment Kit (Pierce) and the eluates of both kits were dried immediately following elution to prevent loss of phosphopeptides due to the high pH. Eluates from both kits were resuspended in basic buffer A (10 mM ammonium hydroxide, pH 10) and were separated into 36 fractions on a 100 x 1.0 mm Acquity BEH C18 column (Waters) using an UltiMate 3000 UHPLC system (Thermo) with a 40 min gradient from 99:1 to 60:40 basic buffer A:B ratio (buffer B: 10 mM ammonium hydroxide, 99.9% acetonitrile, pH 10), and then consolidated into 18 super-fractions.

Multi-Notch MS^3 analysis of TMT-labeled Phosphopeptides
Analysis of TMT-labeled samples were carried out as previously reported [46]. In-line reverse phase fractionation with a Jupiter Proteo resin (Phenomenex) was employed to further reduce the complexity of each super-fraction generated by off-line bHPLC. The resin was packed into a 200 x 0.075 mm column and HPLC was carried out on a Water's nanoAcquity UPLC. A 95-minute gradient was used to elute samples from the reverse phase resin. The gradient consisted of 97:3 to 67:33 Buffer A 0.1% formic acid, 0.5% acetonitrile:B (0.1% formic acid and 99.9% acetonitrile). Electrospray ionization at 2.5 kV was used to ionize eluted peptides into an Obritrap Fusion Lumos Tribrid mass spectrometer (Thermo). Multi-notch MS^3 was used to collect peptide sequence information and TMT-reporter ion quantities. The Orbitrap was used to collect profile MS data over 375 to 1500 m/z at 120,000 resolution. Collision-induced dissociation at 35.0 normalized collision energy fragmented ions for MS/MS. Centroided MS^2 data was collected in the ion trap for ions between 400-2000 m/z. Up to 10 MS^2 ions were selected by SPS, synchronous precursor selection and fragmented by High-energy C-trap dissociation at 65.0 normalized collision energy to separate the TMT-reporter ions from the precursors. Profile MS^3 data from 100-500 m/z was collected at 50,000 within the Orbitrap for quantification of TMT-reporters.

Analysis of phosphopeptides
Phosphopeptides were identified and reporter ions quantified using MaxQuant (Max Planck Institute) with a parent ion tolerance of 3 ppm, a fragment ion tolerance of 0.5 Da, and a reporter ion tolerance of 0.001 Da. Oxidation of methionine and STY phosphorylation were searched as variable modifications, and carbamidomethylation of cysteine residues and TMT-10plex labeling of lysine residues and N-termini of peptides were set as fixed modifications. The data was searched against the human UniProt database UP000005640 (74,458 proteins and added known contaminants). MaxQuant data was further analyzed using R, and the packages LIMMA [47], ggplot2 [48] and heatmaply [49]. A significance criteria of LIMMA Adjusted P-Value < 0.05 and a Log_2 Fold Change of ≥ 1 was employed to produce a "significantly enriched phosphopeptide" list for each groupwise comparison. Pathway analysis was performed on the enriched phosphopeptides for each group using the webtool Enrichr [50] and GO Terms complexity was reduced using REVIGO [51].

Statistics and reproducibility
Quantitative data represent mean ± SEM from at least three independent experiments unless otherwise noted. Two-tailed Student's *t* test was used for statistical analysis by GraphPad Prism 8. Statistical differences were considered significant at $P < 0.05$.

Data Availability Statement

This article does not contain materials or datasets in addition to those included.

Acknowledgement

The authors thank Dr. Roger Greenberg for the U2OS-DSB reporter cell line, Dr. Jing Guo and Faculty Core Facility (The University of Hong Kong) for help with high-content screen, Dr. Wen Deng for advice on preparation of metaphases, Dr. Nabieh Ayoub for the GFP-NELF-A/E constructs, Dr. Jessica Downs for pEGFP-STAG2, Drs. William Hahn and David Root for pDONR223-DYRK1B [52], Dr. Kyle Miller for GFP-BRD7 and GFP-PBRM1 [11], Dr. Thomas Tuschl for RNaseH1 expression construct, Drs. John Doench and David Root for DYRK1B gRNA constructs [53], Dr. Feng Zhang for lentiviral plasmids [54], and Dr. Simon Bekker-Jensen for GFP-53BP1. The work is sponsored by fund from Research Grants Council to MSYH (Project No. C7007-17GF and 17104618) and by National Institute of Health (K22CA204354 & P20GM121293) and Arkansas Breast Cancer Research Program (AWD00053730) to JWCL. XYT is a recipient of the Hong Kong PhD Fellowship and JL is supported by the Lee Shau Kee Postgraduate Fellowship.

Author Contributions

MSYH, SMHS and JWCL conceived and supervised the work. CD performed most experiments with help from XYT and JL. KLW conducted the phospho-proteomic study with supervision and input from JWCL. TI and CHY advised in high-content screen. MSYH, CD, KLW and JWCL prepared the figures for publication. MSYH and CD wrote the manuscript with input from KLW and JWCL. All authors approved of the final version of the manuscript.

Competing Interest Statement

None declared.

References

1. D'Alessandro, G. and F. d'Adda di Fagagna, *Transcription and DNA Damage: Holding Hands or Crossing Swords?* J Mol Biol, 2017. **429**(21): p. 3215-3229.
2. Marnef, A., S. Cohen, and G. Legube, *Transcription-Coupled DNA Double-Strand Break Repair: Active Genes Need Special Care.* J Mol Biol, 2017. **429**(9): p. 1277-1288.
3. Kakarougkas, A., et al., *Requirement for PBAF in transcriptional repression and repair at DNA breaks in actively transcribed regions of chromatin.* Mol Cell, 2014. **55**(5): p. 723-32.
4. Ui, A., Y. Nagaura, and A. Yasui, *Transcriptional elongation factor ENL phosphorylated by ATM recruits polycomb and switches off transcription for DSB repair.* Mol Cell, 2015. **58**(3): p. 468-82.
5. Ji, J.H., et al., *De novo phosphorylation of H2AX by WSTF regulates transcription-coupled homologous recombination repair.* Nucleic Acids Res, 2019.
6. Shanbhag, N.M., et al., *ATM-dependent chromatin changes silence transcription in cis to DNA double-strand breaks.* Cell, 2010. **141**(6): p. 970-81.
7. Pankotai, T., et al., *DNAPKcs-dependent arrest of RNA polymerase II transcription in the presence of DNA breaks.* Nat Struct Mol Biol, 2012. **19**(3): p. 276-82.
8. Caron, P., et al., *WWP2 ubiquitylates RNA polymerase II for DNA-PK-dependent transcription arrest and repair at DNA breaks.* Genes Dev, 2019. **33**(11-12): p. 684-704.
9. Awwad, S.W., et al., *NELF-E is recruited to DNA double-strand break sites to promote transcriptional repression and repair.* EMBO Rep, 2017. **18**(5): p. 745-764.
10. Meisenberg, C., et al., *Repression of Transcription at DNA Breaks Requires Cohesin throughout Interphase and Prevents Genome Instability.* Mol Cell, 2019. **73**(2): p. 212-223 e7.
11. Gong, F., et al., *Screen identifies bromodomain protein ZMYND8 in chromatin recognition of transcription-associated DNA damage that promotes homologous recombination.* Genes Dev, 2015. **29**(2): p. 197-211.
12. de Vivo, A., et al., *The OTUD5-UBR5 complex regulates FACT-mediated transcription at damaged chromatin.* Nucleic Acids Res, 2019. **47**(2): p. 729-746.
13. Sanchez, A., et al., *BMI1-UBR5 axis regulates transcriptional repression at damaged chromatin.* Proc Natl Acad Sci U S A, 2016. **113**(40): p. 11243-11248.
14. Becker, W., *Emerging role of DYRK family protein kinases as regulators of protein stability in cell cycle control.* Cell Cycle, 2012. **11**(18): p. 3389-94.
15. Mercer, S.E. and E. Friedman, *Mirk/Dyrk1B: a multifunctional dual-specificity kinase involved in growth arrest, differentiation, and cell survival.* Cell Biochem Biophys, 2006. **45**(3): p. 303-15.
16. Friedman, E., *Mirk/dyrk1B Kinase in Ovarian Cancer.* Int J Mol Sci, 2013. **14**(3): p. 5560-75.
17. Friedman, E., *The Kinase Mirk/dyrk1B: A Possible Therapeutic Target in Pancreatic Cancer.* Cancers (Basel), 2010. **2**(3): p. 1492-512.
18. Becker, W., *A wake-up call to quiescent cancer cells - potential use of DYRK1B inhibitors in cancer therapy.* FEBS J, 2018. **285**(7): p. 1203-1211.
19. Mazmanian, G., et al., *The zebrafish dyrk1b gene is important for endoderm formation.* Genesis, 2010. **48**(1): p. 20-30.
20. Keramati, A.R., et al., *A form of the metabolic syndrome associated with mutations in DYRK1B.* N Engl J Med, 2014. **370**(20): p. 1909-1919.
21. Coelho, M.C., R.M. Pinto, and A.W. Murray, *Heterozygous mutations cause genetic instability in a yeast model of cancer evolution.* Nature, 2019. **566**(7743): p. 275-278.
22. An, L., et al., *Dual-utility NLS drives RNF169-dependent DNA damage responses.* Proc Natl Acad Sci U S A, 2017. **114**(14): p. E2872-E2881.
23. Tang, J., et al., *Acetylation limits 53BP1 association with damaged chromatin to promote homologous recombination.* Nat Struct Mol Biol, 2013. **20**(3): p. 317-25.
24. Shiloh, Y. and Y. Ziv, *The ATM protein kinase: regulating the cellular response to genotoxic stress, and more.* Nat Rev Mol Cell Biol, 2013. **14**(4): p. 197-210.
25. Lee, K., X. Deng, and E. Friedman, *Mirk protein kinase is a mitogen-activated protein*

kinase substrate that mediates survival of colon cancer cells. Cancer Res, 2000. **60**(13): p. 3631-7.
26. Ashford, A.L., et al., *Identification of DYRK1B as a substrate of ERK1/2 and characterisation of the kinase activity of DYRK1B mutants from cancer and metabolic syndrome.* Cell Mol Life Sci, 2016. **73**(4): p. 883-900.
27. Posavec Marjanovic, M., K. Crawford, and I. Ahel, *PARP, transcription and chromatin modeling.* Semin Cell Dev Biol, 2017. **63**: p. 102-113.
28. Shinkai, Y. and M. Tachibana, *H3K9 methyltransferase G9a and the related molecule GLP.* Genes Dev, 2011. **25**(8): p. 781-8.
29. Wagner, T. and M. Jung, *New lysine methyltransferase drug targets in cancer.* Nat Biotechnol, 2012. **30**(7): p. 622-3.
30. Yang, Q., et al., *G9a coordinates with the RPA complex to promote DNA damage repair and cell survival.* Proc Natl Acad Sci U S A, 2017. **114**(30): p. E6054-E6063.
31. Ginjala, V., et al., *Protein-lysine methyltransferases G9a and GLP1 promote responses to DNA damage.* Sci Rep, 2017. **7**(1): p. 16613.
32. Watanabe, S., et al., *MDC1 methylation mediated by lysine methyltransferases EHMT1 and EHMT2 regulates active ATM accumulation flanking DNA damage sites.* Sci Rep, 2018. **8**(1): p. 10888.
33. Kubicek, S., et al., *Reversal of H3K9me2 by a small-molecule inhibitor for the G9a histone methyltransferase.* Mol Cell, 2007. **25**(3): p. 473-81.
34. Vedadi, M., et al., *A chemical probe selectively inhibits G9a and GLP methyltransferase activity in cells.* Nat Chem Biol, 2011. **7**(8): p. 566-74.
35. Vitor, A.C., et al., *Single-molecule imaging of transcription at damaged chromatin.* Sci Adv, 2019. **5**(1): p. eaau1249.
36. Iacovoni, J.S., et al., *High-resolution profiling of gammaH2AX around DNA double strand breaks in the mammalian genome.* EMBO J, 2010. **29**(8): p. 1446-57.
37. Purman, C.E., et al., *Regional gene repression by DNA double-strand breaks in G1 phase cells.* Mol Cell Biol, 2019.
38. Clouaire, T. and G. Legube, *A Snapshot on the Cis Chromatin Response to DNA Double-Strand Breaks.* Trends Genet, 2019. **35**(5): p. 330-345.
39. Tan, X.Y. and M.S.Y. Huen, *Perfecting DNA double-strand break repair on transcribed chromatin.* Essays Biochem, 2020.
40. Aymard, F., et al., *Genome-wide mapping of long-range contacts unveils clustering of DNA double-strand breaks at damaged active genes.* Nat Struct Mol Biol, 2017. **24**(4): p. 353-361.
41. Lemaitre, C., et al., *Nuclear position dictates DNA repair pathway choice.* Genes Dev, 2014. **28**(22): p. 2450-63.
42. Aymard, F., et al., *Transcriptionally active chromatin recruits homologous recombination at DNA double-strand breaks.* Nat Struct Mol Biol, 2014. **21**(4): p. 366-74.
43. Iannelli, F., et al., *A damaged genome's transcriptional landscape through multilayered expression profiling around in situ-mapped DNA double-strand breaks.* Nat Commun, 2017. **8**: p. 15656.
44. Shimizu, I., et al., *DNA damage response and metabolic disease.* Cell Metab, 2014. **20**(6): p. 967-77.
45. Wessel, D. and U.I. Flugge, *A method for the quantitative recovery of protein in dilute solution in the presence of detergents and lipids.* Anal Biochem, 1984. **138**(1): p. 141-3.
46. Zybailov, B.L., et al., *Metaproteomics reveals potential mechanisms by which dietary resistant starch supplementation attenuates chronic kidney disease progression in rats.* PLoS One, 2019. **14**(1): p. e0199274.
47. Ritchie, M.E., et al., *limma powers differential expression analyses for RNA-sequencing and microarray studies.* Nucleic Acids Res, 2015. **43**(7): p. e47.
48. Wickham, H., *Ggplot2 : elegant graphics for data analysis*. Use R! 2009, New York: Springer. viii, 212 p.
49. Galili, T., et al., *heatmaply: an R package for creating interactive cluster heatmaps for online publishing.* Bioinformatics, 2018. **34**(9): p. 1600-1602.
50. Chen, E.Y., et al., *Enrichr: interactive and collaborative HTML5 gene list enrichment*

analysis tool. BMC Bioinformatics, 2013. **14**: p. 128.
51. Supek, F., et al., *REVIGO summarizes and visualizes long lists of gene ontology terms.* PLoS One, 2011. **6**(7): p. e21800.
52. Johannessen, C.M., et al., *COT drives resistance to RAF inhibition through MAP kinase pathway reactivation.* Nature, 2010. **468**(7326): p. 968-72.
53. Doench, J.G., et al., *Optimized sgRNA design to maximize activity and minimize off-target effects of CRISPR-Cas9.* Nat Biotechnol, 2016. **34**(2): p. 184-191.
54. Sanjana, N.E., O. Shalem, and F. Zhang, *Improved vectors and genome-wide libraries for CRISPR screening.* Nat Methods, 2014. **11**(8): p. 783-784.

Figure Legends

Figure 1 Chemical screen identifies novel regulators of transcription at DSBs
A) Schematic illustration of DISC reporter in U2OS-DSB reporter cell. Doxycycline (Dox) induces nascent transcription and local YFP-MS2 accumulation at transgene locus. Cell treatment with 4-OHT and Shield-1 leads to FokI-induced DSBs and suppression of proximal transcription; **B**) Workflow depicting kinase inhibitor library screen using U2OS-DSB reporter cells. DSB-induced cells pre-treated with each of the 760 kinase inhibitors were subjected to high-content imaging and automated analyses for YFP-MS2 focus; **C**) Ranking of nuclear kinase inhibitor targets with putative role in transcription silencing; **D**) FokI-induced DSBs silence transcription in control but not in ATM- or DYRK1B-inhibited cells. Expression of FokI wildtype (WT) but not its catalytically-inactive mutant (D450A) suppressed doxycycline-induced transcription. Pre-treatment with ATM inhibitor (ATMi; KU55933) or DYRK1B inhibitor (DYRK1Bi; AZ191) attenuated DSB-induced transcription silencing. U2OS-DSB reporter cells grown on coverslips were transfected with either FokI WT or D450A expression construct. 24 hr post-transfection cell were PFA-fixed and processed for fluorescence imaging; **E**) ATM and DYRK1B act epistatically to mount DISC. U2OS-DSB reporter cells pretreated with DMSO or indicated inhibitor(s) were induced with 4-OHT and Shield-1. Relative mean fluorescence intensity (MFI) of YFP-MS2 foci is shown and bars represent mean ± SEM; $^{****}P<0.0001$; ns, not significant.

Figure 2 DYRK1B promotes DSB-induced transcription silencing
A) U2OS-DSB reporter cell transfected with control (siCTR) or DYRK1B-specific siRNAs (siDYRK1B-1 and siDYRK1B-2) were induced with Dox, 4-OHT and Shield-1 for 3 hours. Cells were processed for fluorescence imaging to quantify mean fluorescence intensity (MFI) of YPF-MS2 or Western blotting experimentations using indicated antibodies. Bars represent mean ± SEM; $^{***}P<0.001$, $^{****}P<0.0001$; **B**) Schematic illustration of 5-EU incorporation experiment to analyse nascent transcription; **C**) HeLa cells transfected with control (siCTR) or DYRK1B-specific siRNAs (siDYRK1B-1 and siDYRK1B-2) were processed for laser microirradiation. Fixed cells were labeled for 5-EU and γH2AX. Nucleic were counterstained with DAPI. Representative images and quantification of relative 5-EU fluorescence intensity are shown. Western blotting using indicated antibodies was performed to evaluate RNAi-depletion of DYRK1B; **D**) U2OS-DSB reporter cells pre-treated with indicated siRNAs were transfected with Myc vector or Myc-tagged DYRK1B wildtype (WT) and kinase mutants (K140M or D239A). Cells were processed 24 hr post-transfection as in (**A**) and YFP-MS2 foci were analysed and quantified. Western blotting experimentations were performed to evaluate expression of Myc-DYRK1B alleles. Bars represent mean ± SEM; $^{***}P<0.001$, $^{****}P<0.0001$; ns, not significant.

Figure 3 DYRK1B is recruited to laser-induced DSBs
A) Cells expressing GFP-DYRK1B or GFP alone were laser microirradiated and time-lapse images were captured to analyse protein accumulation at DNA damage tracks. Quantification of GFP-DYRK1B or GFP accumulation at DSBs was performed. Arrowheads denote sites of laser microirradiation; **B - C**) Schematics and steady state expression level of DYRK1B and its deletion mutant are shown. NLS, Nuclear Localisation Signal; KD, Kinase Domain; PEST, the proline, glutamic acid, serine and threonine rich domain; **D - E**) U2OS cells expressing GFP-DYRK1B or mutants (see **Panel B**) were laser microirradiated. Representative images from pre-damaged and laser-damaged (100 sec post microirradiation) cells are shown; **F - G**) U2OS cells expressing GFP-DYRK1B were pre-treated with indicated inhibitors prior to laser microirradiation. Cells were processed as in (**A**) and representative images are shown as in (**D**).

Figure 4 DYRK1B facilitates repair of IR-induced DNA damage
A) DYRK1B-silenced cells reconstituted with Dox-inducible expression vector (TRE-Vector-Flag) or those that harbour DYRK1B alleles were induced with doxycycline. 24 hr post treatment cells were irradiated and allowed to recover. Cells were thereafter processed for the Comet assay according to standard procedures. Relative tail moment of at least 200 cells from two independent experiments were quantified using Image J and results were plotted. Western blotting was performed to examine expression of DYRK1B using indicated antibodies. Asterisk denotes protein band that corresponds to endogenous DYRK1B. Bars represent mean ± SEM;

$^{****}P<0.0001$; **B**) Representative metaphase preparations from IR-treated HeLa derivatives are shown. HeLa cells lenti-virally infected with DYRK1B gRNA (DYRK1B gRNA#1) were reconstituted with vector or DYRK1B alleles. Cells were thereafter irradiated and processed to determine the number of chromosomal breaks. At least 120 metaphases from two independent experiments were counted and results were plotted. Bars represent mean ± SEM; $^{*}P<0.05$, $^{****}P<0.0001$; **C**) Scheme depicting cell processing for neutral Comet assay following transient global inhibition of transcription using DRB; **D**) Western blotting was performed to evaluate expression of DYRK1B; **E**) Representative images from single cell electrophoresis to analyse relative tail moment. Quantification is shown and was derived from at least 200 cells from two independent experiments. Bars represent mean ± SEM; $^{***}P<0.001$, $^{****}P<0.0001$; ns, not significant; **F**) Scheme depicting cell processing for metaphase analyses following transient global inhibition of transcription using DRB; **G**) Representative metaphase preparations from IR-treated HeLa derivatives are shown. Number of chromosomal breaks were quantified in HeLa cells processed as in (B) with or without pre-DRB treatment. Bars represent mean ± SEM; $^{*}P<0.05$, $^{**}P<0.01$; ns, not significant.

Figure 5 Global phospho-proteomic identification of DYRK1B substrates
A) Schematic diagram of phospho-proteomic analysis using high resolution mass spectrometry; **B**) Heatmap expressing the different relative abundances of phosphopeptides between parental cells, DYRK1B overexpression (OE) cells, and DYRK1B knockout (KO) cells; **C**) DYRK1B phosphorylation motif determined from the significantly-enriched phosphopeptides in overexpression (OE) vs knockout (KO) samples; **D**) Top biological process GO:Terms related to transcription within the total top 50 terms as determined by EnrichR comparing overexpression (OE) vs knockout (KO) cell lines. Size of data points signifies number of significant proteins within each pathway. Data represents 4 biological replicates; **E**) RNAi-based validation screen for DYRK1B targets in DISC. U2OS-DSB reporter cells pre-treated with indicated siRNA pools were induced with Dox, 4-OHT and Shield-1. Cells were thereafter processed to visualize mCherry-FokI and YFP-MS2 foci.

Figure 6 EHMT2 promotes transcription silencing on damaged chromatin
A) EHMT2 inactivation compromised DSB-induced transcription silencing. U2OS-DSB reporter cells lenti-virally transduced with indicated gRNAs were incubated with Dox, 4-OHT and Shield-1 to induce DSBs proximal to transcription unit. Thereafter cells were processed to visualise YFP-MS2 and mCherry-FokI foci. Nuclei were counterstained with DAPI. Mean fluorescence intensity (MFI) of YFP-MS2 was quantified. Bars represent mean ± SEM; $^{****}P<0.0001$; ns, not significant. Western blotting was performed to evaluate expression of EHMT2; **B**) EHMT2 silencing led to sustained nascent transcription at laser-induced DSBs. HeLa cells transduced with indicated gRNAs were laser microirradiated. Cells were processed 1 hour after to evaluate 5-EU incorporation at laser-induced DNA damage tracks. Quantification of 5-EU incorporation at laser-induced γH2AX-marked DSBs was performed. Data represents mean ± SEM from three independent experiments. Western blotting was performed to evaluate expression of EHMT2; **C - D**) Chemical inhibition of EHMT2 attenuated DISC. Cells pre-treated with either ATM inhibitor (KU55933) or EHMT2 inhibitor (UNC0638) were processed for visualisation of mCherry-FokI and YFP-MS2 (**C**) or 5-EU incorporation assay (**D**). Representative images are shown. Arrowheads denote YFP-MS2 focus or anti-5-EU stripes. Data represents mean ± SEM from three independent experiments; **E - F**) Genetic inactivation of EHMT2 methyltransferase activity compromised transcription silencing proximal to FokI- (**E**) and laser-induced (**F**) DSBs. Control gRNA- or EHMT2 gRNA-targeted cells reconstituted with vector control, wildtype (WT) EHMT2 or its SET deletion mutant (ΔSET) were subjected to either the U2OS-DSB reporter assay as in (**A**) or the 5-EU incorporation assay as in (**B**). Quantification and Western blotting analyses were performed as in (**A**) and (**B**). Note that the EHMT2 antibodies were raised against a synthetic peptide corresponding to the carboxy terminus of the protein, and do not recognise the EHMT2 SET-deletion mutant.

Figure 7 DYRK1B facilitates EHMT2 recruitment to DSBs
A) Control (CTR gRNA) or cells transduced with DYRK1B gRNAs (DYRK1B gRNA#1 and DYRK1B gRNA#2) were transiently transfected with GFP-EHMT2 expression construct. 24 hr post transfection cells were microirradiated and time-lapse images were captured to monitor GFP-

EHMT2 migration to laser-induced DNA damage tracks. Quantification is shown and is derived from two independent experiments of at least 10 cells each; **B**) Schematic illustration of EHMT2 protein domains and the DYRK1B-enriched EHMT2 phospho-peptide surrounding T346. Note that T346 corresponds to T555 in the long isoform of EHMT2; **C - D**) GFP-tagged wildtype (WT) EHMT2 or its phospho-mutants (T346A and T346D) were expressed in U2OS cells prior to laser microirradiation and time-lapse imaging experimentations as done in (**A**); **E**) Working model depicting DYRK1B in orchestrating transcription suppressing on DSB-flanking chromatin. DYRK1B accumulates at DSBs in a PARP-dependent manner, and promotes EHMT2 T346 phosphorylation and concentration at DSBs to effect DISC.

A

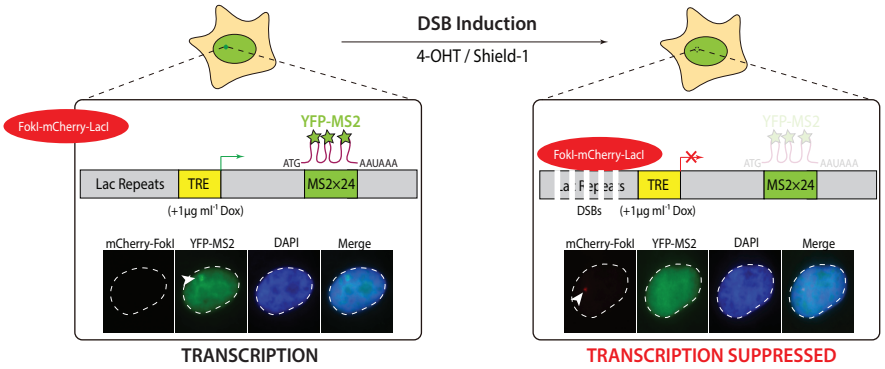

B

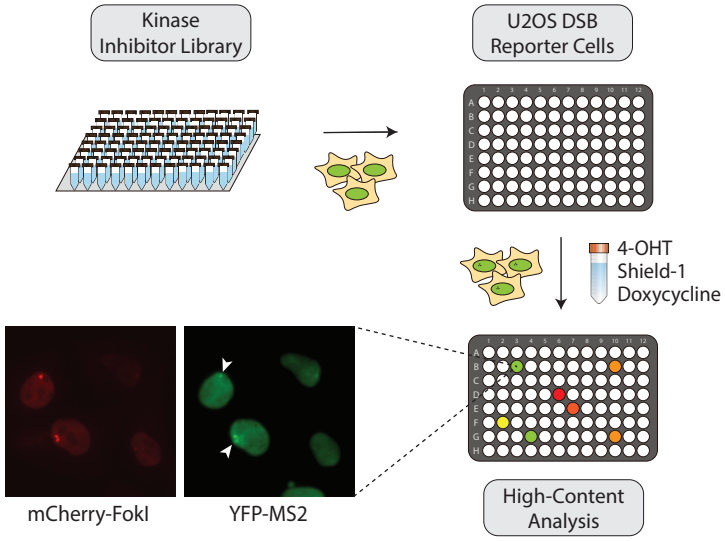

C

Rank	Target	%YFP Postive cells
1	ATM/ATR	40-49%
2	CDK	30-39%
	DNA-PK	
3	PI3K	25-29%
	p38 MAPK	
	GSK3	
	LRRK2	
	CHK1	
	FGFR	
	ERK	
	JAK	
	RAF	
	DYRK1B	
	PDGFR	
4	AKT	20-24%
	CK2	
	Aurora	
	ALK2	
	p70S6K	
	Bcr-Abl	
	PDK1	
	NUAK	
	CLK	
	WEE1	
5	EP300	18-19%
	IRS1/2	
	MNK1/2	
	PTEN	
	CDC7	
	CHK2	
	PDK	

D

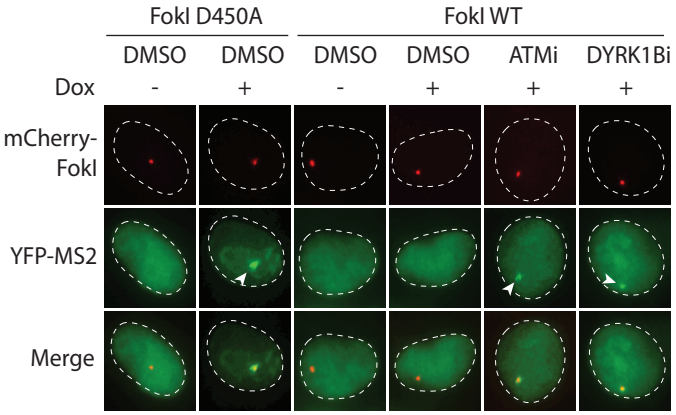

E

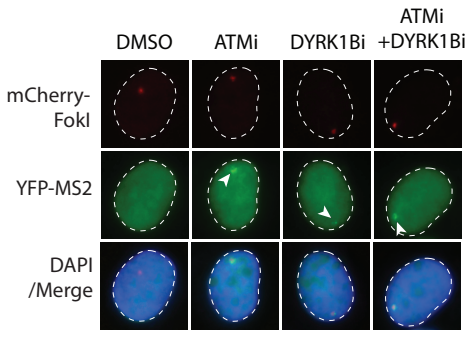

Figure 2

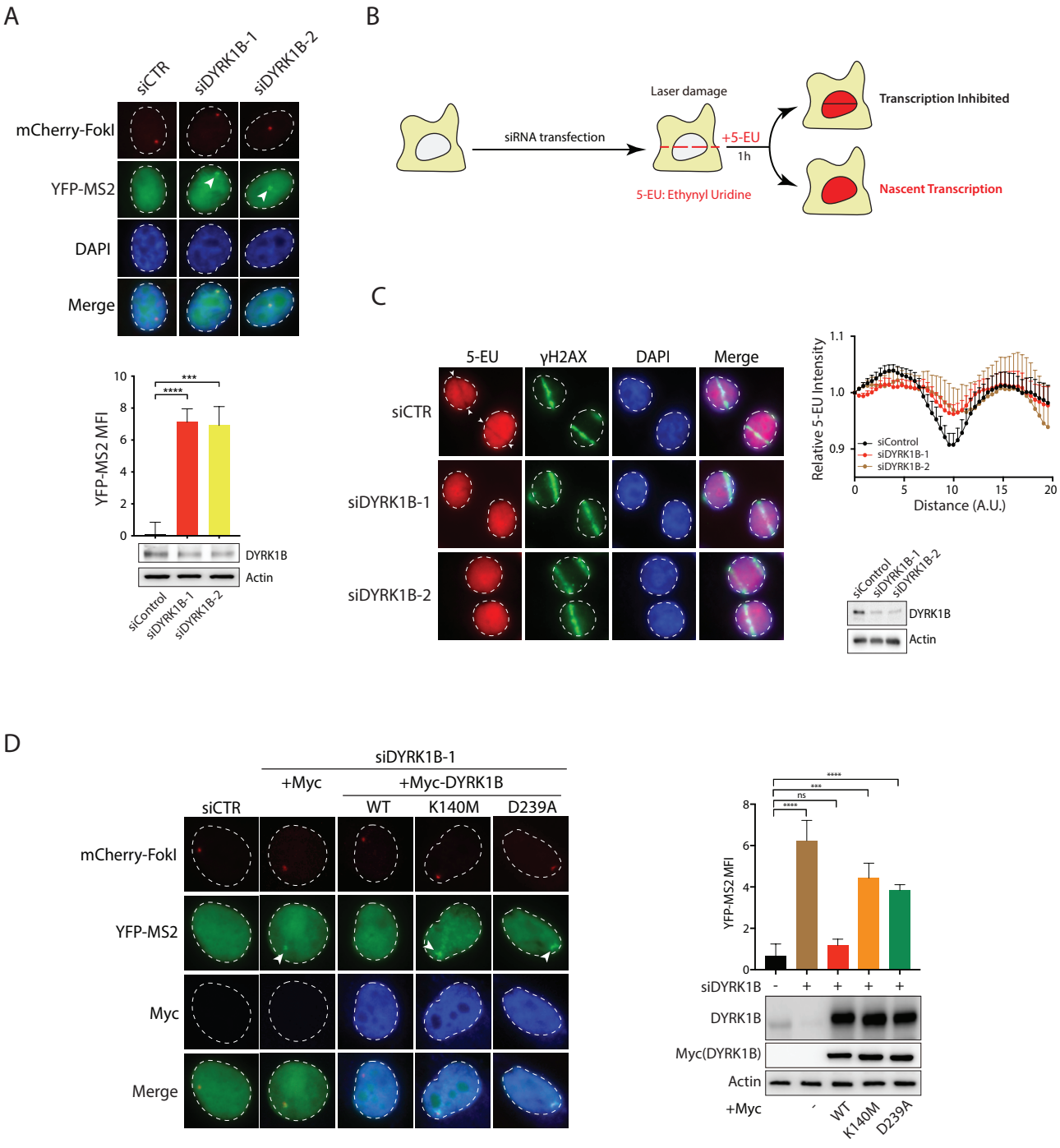
A
siCTR
siDYRK1B-1
siDYRK1B-2
mCherry-FokI
YFP-MS2
DAPI
Merge
YFP-MS2 MFI
***
****
DYRK1B
Actin
siControl
siDYRK1B-1
siDYRK1B-2
B
siRNA transfection
Laser damage
+5-EU
1h
5-EU: Ethynyl Uridine
Transcription Inhibited
Nascent Transcription
C
5-EU
γH2AX
DAPI
Merge
siCTR
siDYRK1B-1
siDYRK1B-2
Relative 5-EU Intensity
siControl
siDYRK1B-1
siDYRK1B-2
Distance (A.U.)
DYRK1B
Actin
D
siDYRK1B-1
+Myc
+Myc-DYRK1B
siCTR
WT
K140M
D239A
mCherry-FokI
YFP-MS2
Myc
Merge
ns
YFP-MS2 MFI
siDYRK1B
DYRK1B
Myc(DYRK1B)
Actin
+Myc
WT
K140M
D239A

Figure 3

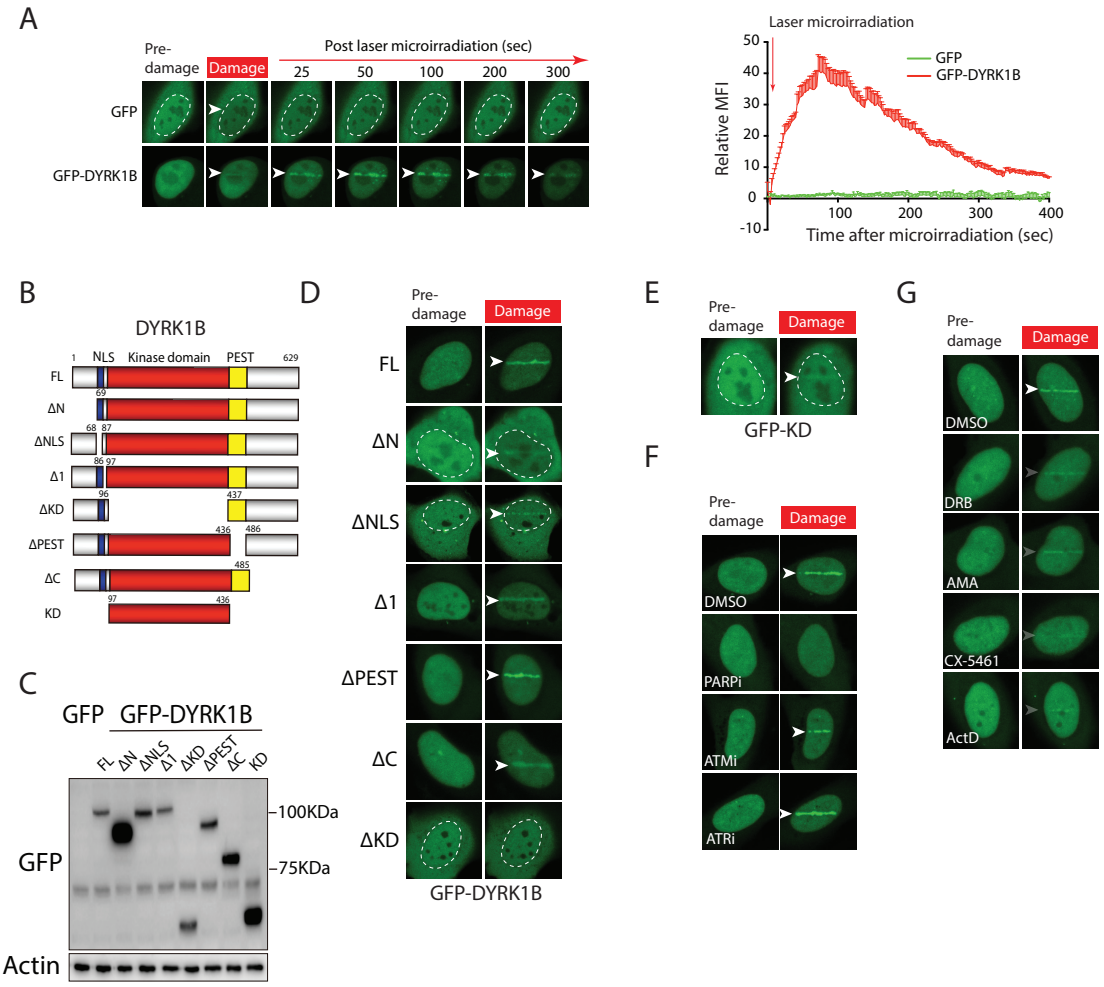
A
Pre-damage
Damage
Post laser microirradiation (sec)
25
50
100
200
300
GFP
GFP-DYRK1B
Laser microirradiation
Relative MFI
GFP
GFP-DYRK1B
Time after microirradiation (sec)
B
DYRK1B
NLS
Kinase domain
PEST
FL
ΔN
ΔNLS
Δ1
ΔKD
ΔPEST
ΔC
KD
C
GFP
GFP-DYRK1B
100KDa
75KDa
Actin
D
GFP-DYRK1B
E
GFP-KD
F
DMSO
PARPi
ATMi
ATRi
G
DMSO
DRB
AMA
CX-5461
ActD

A

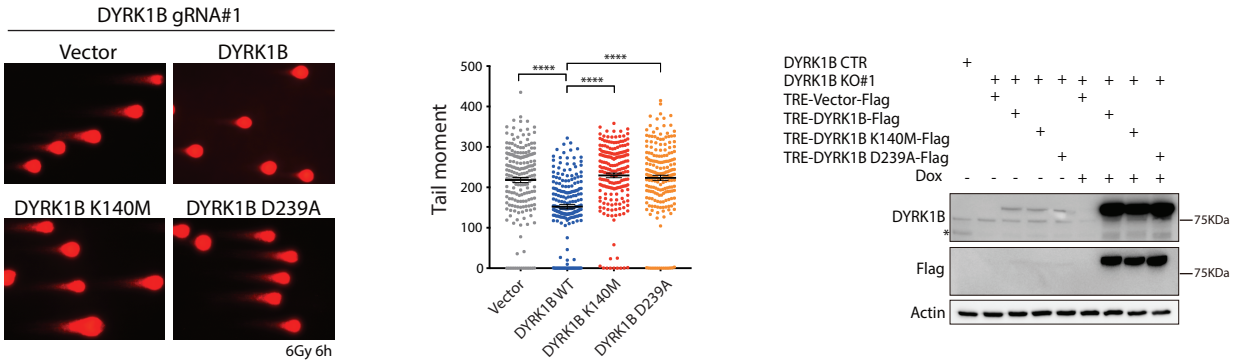
DYRK1B gRNA#1
Vector
DYRK1B
DYRK1B K140M
DYRK1B D239A
6Gy 6h
Tail moment
Vector
DYRK1B WT
DYRK1B K140M
DYRK1B D239A
DYRK1B CTR
DYRK1B KO#1
TRE-Vector-Flag
TRE-DYRK1B-Flag
TRE-DYRK1B K140M-Flag
TRE-DYRK1B D239A-Flag
Dox
DYRK1B
Flag
Actin
75KDa

B

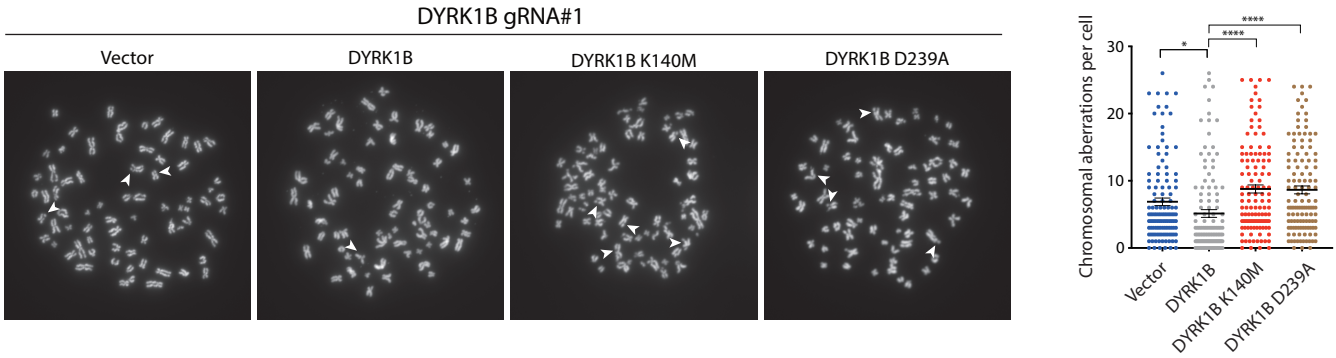
DYRK1B gRNA#1
Vector
DYRK1B
DYRK1B K140M
DYRK1B D239A
Chromosomal aberrations per cell
Vector
DYRK1B
DYRK1B K140M
DYRK1B D239A

C

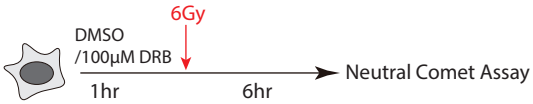
DMSO
/100μM DRB
6Gy
1hr
6hr
Neutral Comet Assay

D

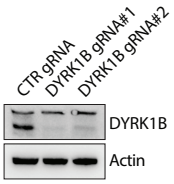
CTR gRNA
DYRK1B gRNA#1
DYRK1B gRNA#2
DYRK1B
Actin

E

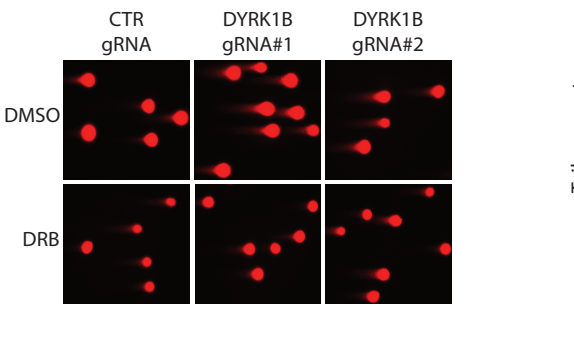
CTR gRNA
DYRK1B gRNA#1
DYRK1B gRNA#2
DMSO
DRB
Tail moment
DRB
CTR gRNA
DYRK1B gRNA#1
DYRK1B gRNA#2

F

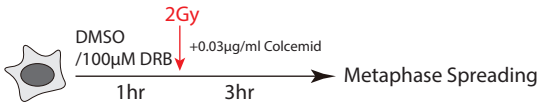
DMSO
/100μM DRB
2Gy
+0.03μg/ml Colcemid
1hr
3hr
Metaphase Spreading

G

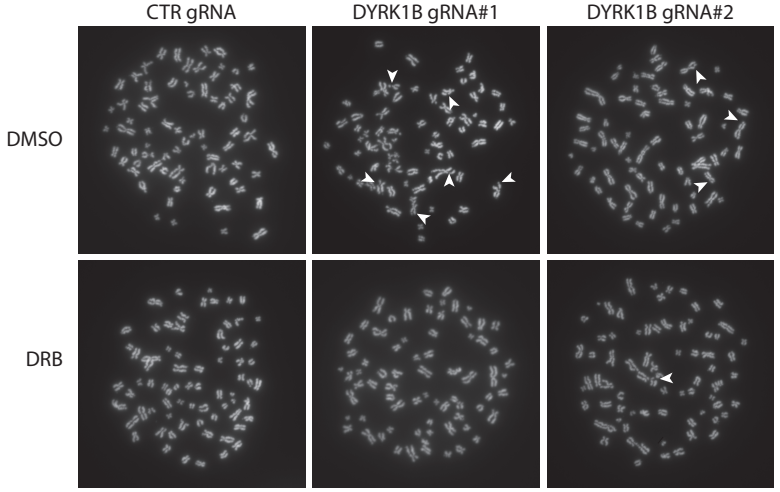
CTR gRNA
DYRK1B gRNA#1
DYRK1B gRNA#2
DMSO
DRB
Chromosomal aberrations per cell
DRB
CTR gRNA
DYRK1B gRNA#1
DYRK1B gRNA#2

Figure 5

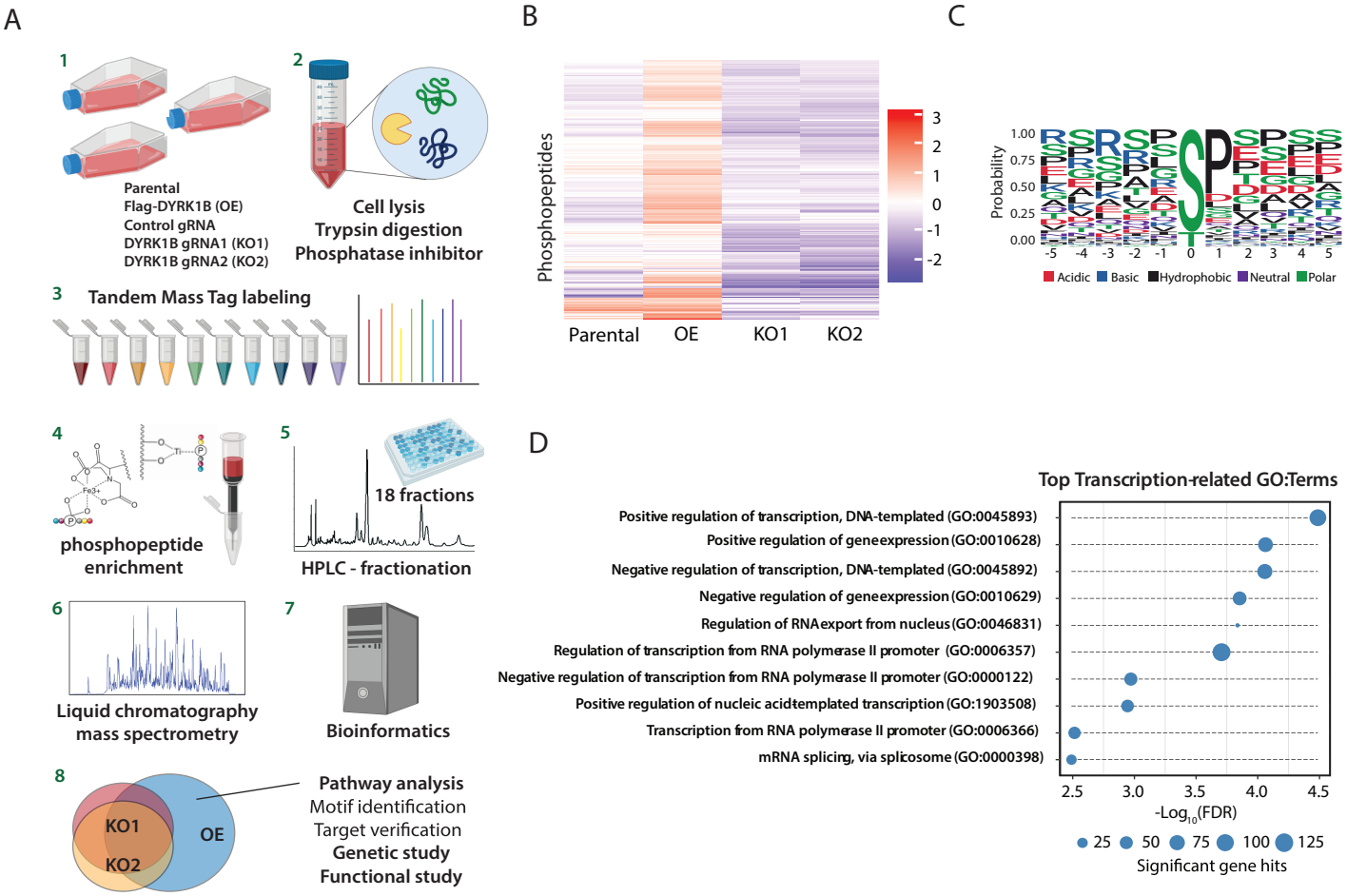
A
1
Parental
Flag-DYRK1B (OE)
Control gRNA
DYRK1B gRNA1 (KO1)
DYRK1B gRNA2 (KO2)
2
Cell lysis
Trypsin digestion
Phosphatase inhibitor
3
Tandem Mass Tag labeling
4
phosphopeptide enrichment
5
18 fractions
HPLC - fractionation
6
Liquid chromatography mass spectrometry
7
Bioinformatics
8
KO1
KO2
OE
Pathway analysis
Motif identification
Target verification
Genetic study
Functional study
B
Phosphopeptides
Parental
OE
KO1
KO2
3
2
1
0
-1
-2
C
Probability
1.00
0.75
0.50
0.25
0.00
-5 -4 -3 -2 -1 0 1 2 3 4 5
Acidic
Basic
Hydrophobic
Neutral
Polar
D
Top Transcription-related GO:Terms
Positive regulation of transcription, DNA-templated (GO:0045893)
Positive regulation of gene expression (GO:0010628)
Negative regulation of transcription, DNA-templated (GO:0045892)
Negative regulation of gene expression (GO:0010629)
Regulation of RNA export from nucleus (GO:0046831)
Regulation of transcription from RNA polymerase II promoter (GO:0006357)
Negative regulation of transcription from RNA polymerase II promoter (GO:0000122)
Positive regulation of nucleic acid-templated transcription (GO:1903508)
Transcription from RNA polymerase II promoter (GO:0006366)
mRNA splicing, via spliceosome (GO:0000398)
2.5 3.0 3.5 4.0 4.5
-Log10(FDR)
25 50 75 100 125
Significant gene hits

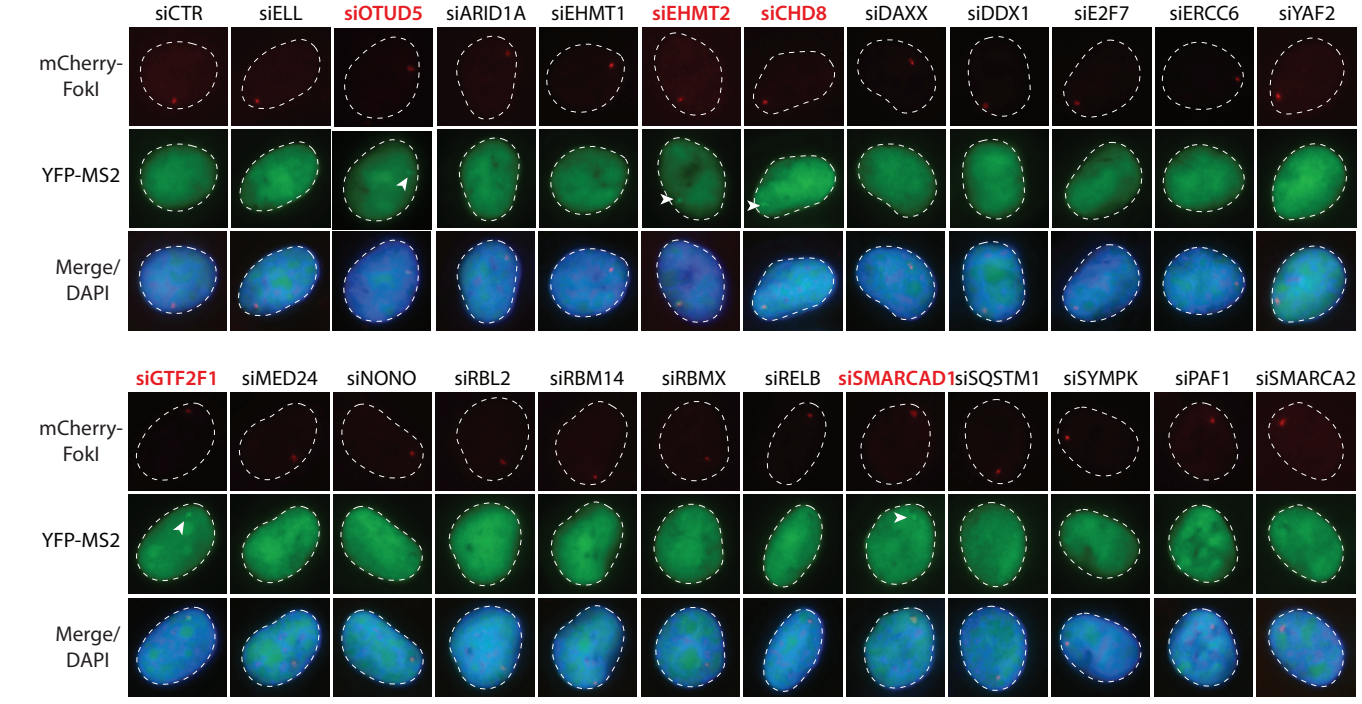
E
siCTR
siELL
siOTUD5
siARID1A
siEHMT1
siEHMT2
siCHD8
siDAXX
siDDX1
siE2F7
siERCC6
siYAF2
mCherry-FokI
YFP-MS2
Merge/ DAPI
siGTF2F1
siMED24
siNONO
siRBL2
siRBM14
siRBMX
siRELB
siSMARCAD1
siSQSTM1
siSYMPK
siPAF1
siSMARCA2
mCherry-FokI
YFP-MS2
Merge/ DAPI

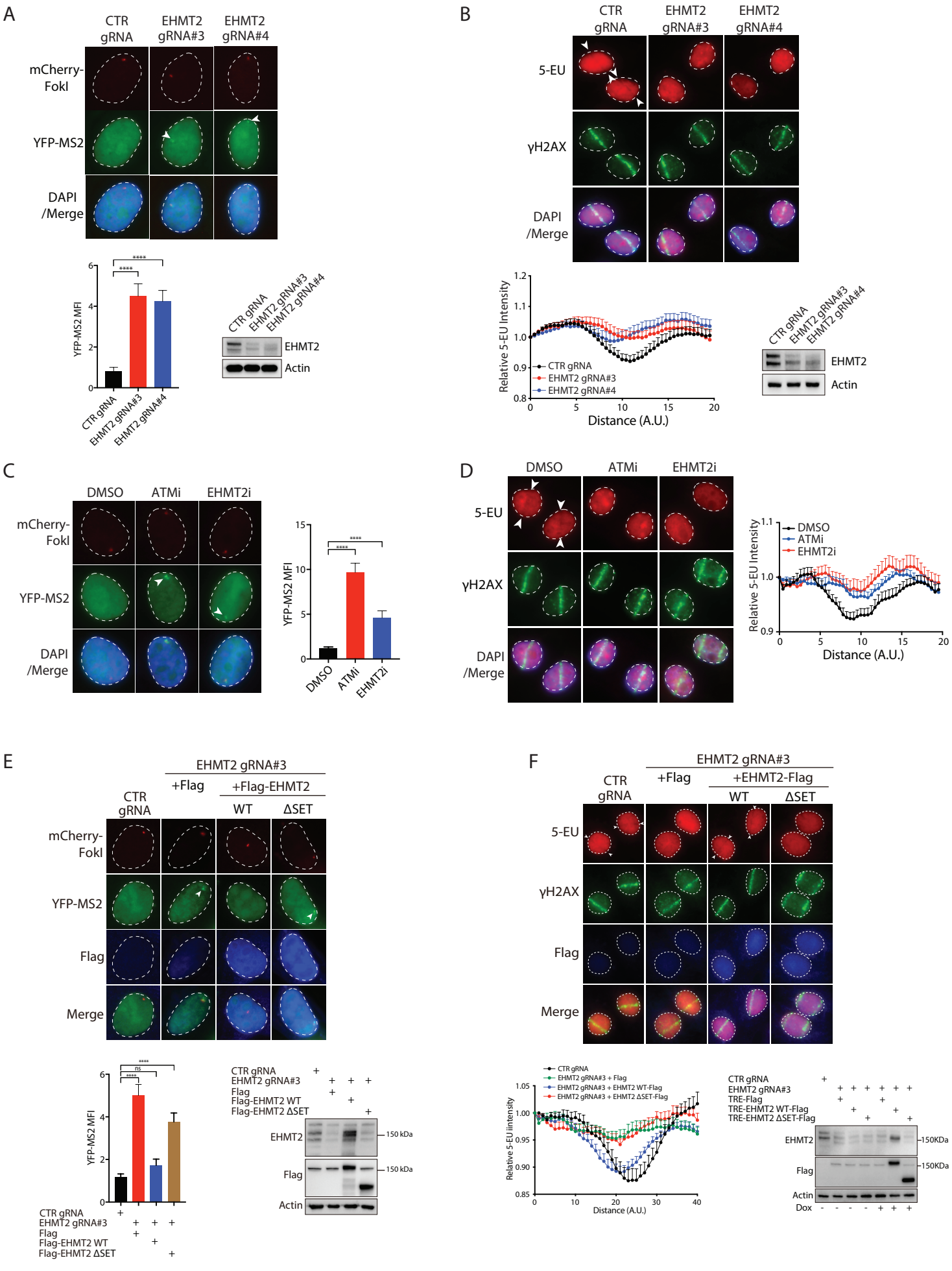
A
CTR gRNA
EHMT2 gRNA#3
EHMT2 gRNA#4
mCherry-FokI
YFP-MS2
DAPI /Merge
YFP-MS2 MFI
EHMT2
Actin
B
5-EU
γH2AX
Relative 5-EU Intensity
Distance (A.U.)
C
DMSO
ATMi
EHMT2i
D
E
+Flag
+Flag-EHMT2
WT
ΔSET
Flag
Merge
Flag-EHMT2 WT
Flag-EHMT2 ΔSET
150 kDa
F
+EHMT2-Flag
TRE-Flag
TRE-EHMT2 WT-Flag
TRE-EHMT2 ΔSET-Flag
Dox
150KDa

A

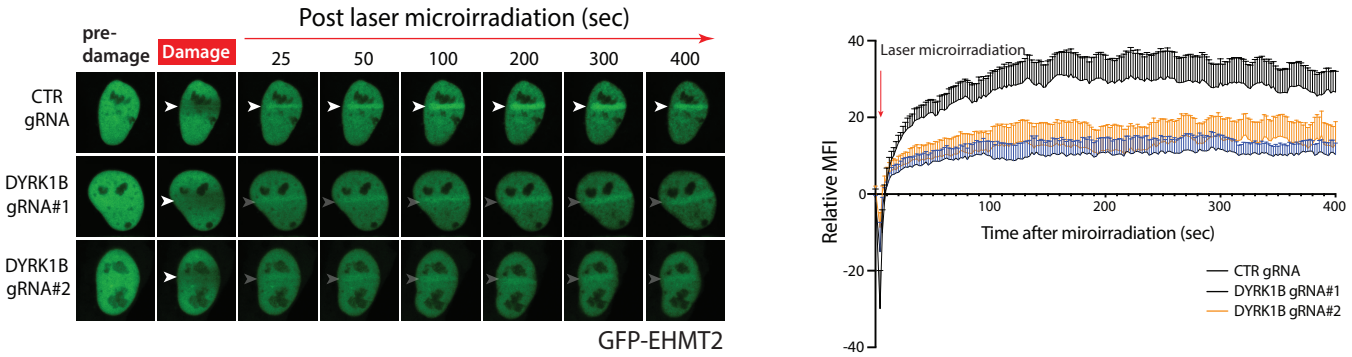
Post laser microirradiation (sec)
pre-damage
Damage
25
50
100
200
300
400
CTR gRNA
DYRK1B gRNA#1
DYRK1B gRNA#2
GFP-EHMT2
Laser microirradiation
Relative MFI
Time after miroirradiation (sec)
CTR gRNA
DYRK1B gRNA#1
DYRK1B gRNA#2

B

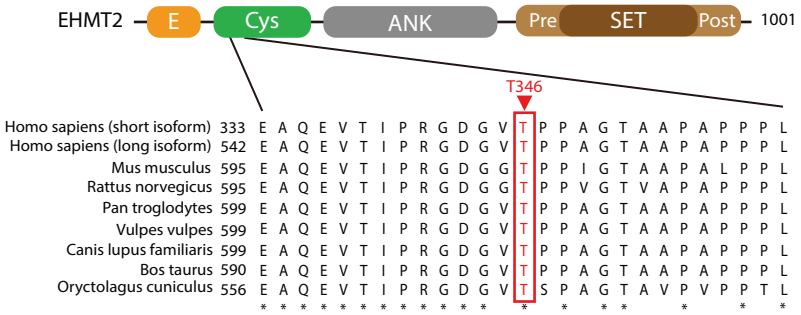
EHMT2
E
Cys
ANK
Pre
SET
Post
1001
T346
Homo sapiens (short isoform) 333 E A Q E V T I P R G D G V T P P A G T A A P A P P P L
Homo sapiens (long isoform) 542 E A Q E V T I P R G D G V T P P A G T A A P A P P P L
Mus musculus 595 E A Q E V T I P R G D G G T P P I G T A A P A L P P L
Rattus norvegicus 595 E A Q E V T I P R G D G G T P P V G T V A P A P P P L
Pan troglodytes 599 E A Q E V T I P R G D G V T P P A G T A A P A P P P L
Vulpes vulpes 599 E A Q E V T I P R G D G V T P P A G T A A P A P P P L
Canis lupus familiaris 599 E A Q E V T I P R G D G V T P P A G T A A P A P P P L
Bos taurus 590 E A Q E V T I P R G D G V T P P A G T A A P A P P P L
Oryctolagus cuniculus 556 E A Q E V T I P R G D G V T S P A G T A V P V P P T L

C

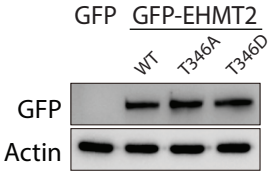
GFP
GFP-EHMT2
WT
T346A
T346D
GFP
Actin

D

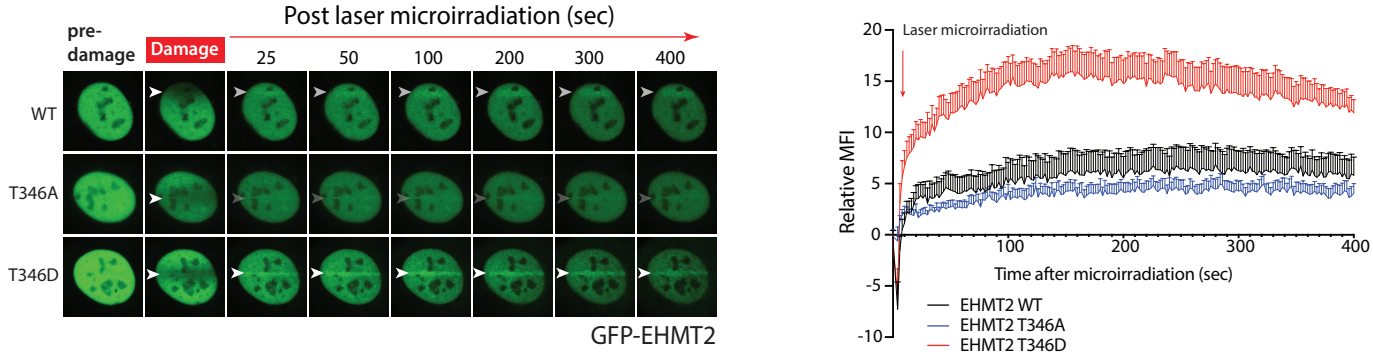
Post laser microirradiation (sec)
pre-damage
Damage
25
50
100
200
300
400
WT
T346A
T346D
GFP-EHMT2
Laser microirradiation
Relative MFI
Time after microirradiation (sec)
EHMT2 WT
EHMT2 T346A
EHMT2 T346D

E

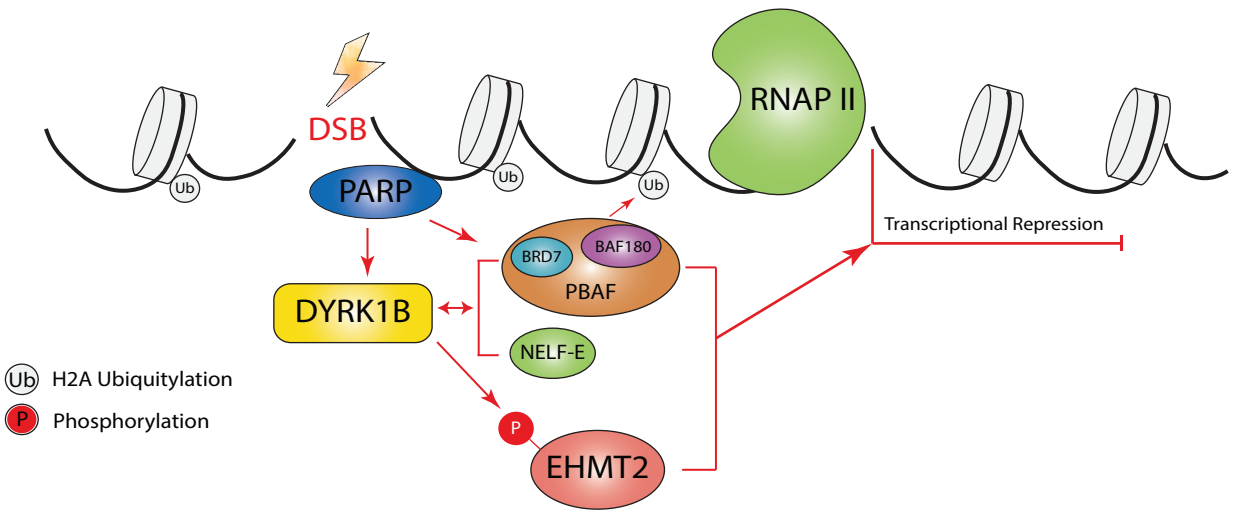
DSB
PARP
RNAP II
Ub
BRD7
BAF180
PBAF
DYRK1B
NELF-E
P
EHMT2
Transcriptional Repression
Ub H2A Ubiquitylation
P Phosphorylation